

## Microstereolithography of Tissue Scaffolds Using a Biodegradable Photocurable Polyester

Nicholas A. Chartrain<sup>1,4</sup>, Maria Vratsanos<sup>2</sup>, Dung T. Han<sup>1</sup>, Justin M. Serrine<sup>3,4</sup>, Allison Pekkanen<sup>3,4</sup>, Timothy E. Long<sup>3,4</sup>, Abby R. Whittington<sup>1,4</sup>, Christopher B. Williams<sup>2,4</sup>

<sup>1</sup>Department of Materials Science & Engineering, Virginia Tech, Blacksburg, VA 24061

<sup>2</sup>Department of Mechanical Engineering, Virginia Tech, Blacksburg, VA 24061

<sup>3</sup>Department of Chemistry, Virginia Tech, Blacksburg, VA 24061

<sup>4</sup>Macromolecules and Interfaces Institute, Virginia Tech, Blacksburg, VA 24061

Correspondence: Nicholas Chartrain nickchar@vt.edu

Keywords: Tissue Scaffold, Regenerative Medicine, Stereolithography, Biodegradable, Polymer

### Abstract

Due to its ability to create complex cellular geometries with extremely fine resolution, mask projection microstereolithography (MP $\mu$ SL) can be useful for fabricating designed tissue scaffolds and other biological constructs for use in Tissue Engineering and Regenerative Medicine. However, few photocurable materials with low cytotoxicity, adequate cell adhesion, and degradability can be processed with MP $\mu$ SL. In this work, we present the fabrication of biocompatible and biodegradable tissue scaffolds with 50  $\mu$ m feature sizes from a novel polyester using MP $\mu$ SL. Poly(tri(ethylene glycol)adipate) dimethacrylate (PTEGA-DMA) was synthesized and evaluated for its printability. The curing parameters for printing were identified and scaffolds were fabricated. Optical and electron microscopy were used to determine the achievable feature sizes and accuracy of printed parts using the polymer in the MP $\mu$ SL system. MC3T3-E1 mouse preosteoblasts were seeded on PTEGA-DMA films to assess adhesion and biocompatibility.

### 1. Introduction

#### 1.1. The Need for Tissue Scaffolds

Millions of patients suffer from damaged or diseased tissue resulting from a wide variety of diseases, conditions, and accidents. Current treatments generally consist of using drugs, wound dressings or biomedical devices to alleviate symptoms, but do not replace or repair damaged tissue with healthy tissue [1, 2]. Thousands of patients receive transplant tissues and organs each year, but others must wait many years before a transplant becomes available [3]. For many other conditions, using transplant tissue is not practical. Patients suffering from diabetic foot ulcers, skin burns and wounds, organ failure, and bone fractures would benefit from a greater availability and variety of replacement tissue.

Tissue Engineering aims to use tissue scaffolds in conjunction with cells as well as chemical, mechanical, or electrical stimuli to construct functional tissue that can be used to repair or replace damaged or diseased tissues [1, 2, 4, 5]. Tissue scaffolds are sponge or network-like devices that provide a three-dimensional environment upon which cells can attach, grow, and proliferate [6]. Scaffolds must maintain sufficient porosity for nutrients to flow into the scaffolds

while also providing structural support for the cells [7]. Fulfilling these two goals requires creative scaffold design as structures with greater porosities tend to have less mechanical strength. In addition, the incorporation of biochemical factors into tissue scaffolds, such as growth factors, small molecules, or even minerals, can significantly enhance cell adhesion, viability, and differentiation [8-10]. Mechanical exercising and electrical stimulation of certain cell types has also been shown to improve cell differentiation and function [11]. Finally, tissue scaffolds require vascularization, or the incorporation of a system for blood flow throughout the scaffold. While many have reported tissue scaffolds that provide mechanical robustness, adequate porosity, and the incorporation of chemical factors, success at incorporating vascularization into tissue scaffolds has been limited [12, 13]. Creating the foundation for a vascular system in a tissue scaffold is undoubtedly the greatest challenge in Tissue Engineering and has hindered the fabrication of large tissue scaffolds for the replacement of solid tissues and organs [13, 14].

## 1.2. Benefits of AM in Fabricating Tissue Scaffolds

Tissue scaffolds resulting from traditional manufacturing techniques feature stochastic distribution of pores. Specifically, these techniques such as gas foaming, particulate leeching, and electrospinning (**Figure 1**) have the ability to control pore size and density, but pore placement occurs randomly within the scaffold [15]. The lack of ability to control the precise mesostructure of the scaffold affects the repeatability of the process, and makes it very difficult to incorporate vasculature into the structure [13, 14]. Without vasculature, cells that migrate to the center of the tissue scaffold will not have sufficient access to nutrients provided by blood [13]. Such scaffolds feature healthy cells on the surface, while apoptosis, programmed cell death, occurs in the center of the scaffold.

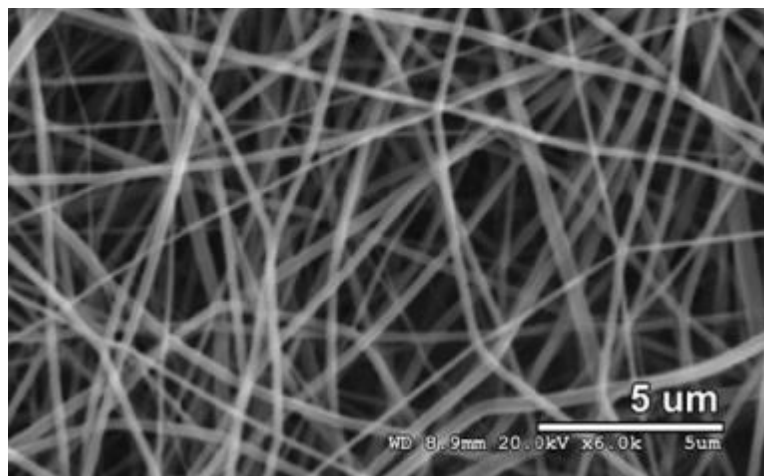


**Figure 1.** Electrospun scaffold used for tissue engineering [16].

Additive Manufacturing systems, often referred to as 3D printers, have the ability to precisely control material placement in three dimensional space [17]. This allows 3D printers to repeatedly fabricate complex designed structures that could not be fabricated by other means. The ability of 3D printers to construct complex geometries with designed macro and mesostructure makes them ideal for fabricating tissue scaffolds that incorporate vasculature [18-21].

### 1.3. Advantages of Mask Projection Microstereolithography

While all AM systems are able to fabricate complex designed structures, some are more suited for fabricating tissue scaffolds than others. The AM system chosen should be able to fabricate features with sizes on the order of a cell diameter ( $\sim 10\ \mu\text{m}$ ) so that surface area of the tissue scaffold can be maximized [6]. Achieving such fine features has proven difficult with most AM systems [17]. The printed resolution of techniques such as filament-based extrusion and Powder Bed Fusion are limited by extrusion tip diameter, powder particle size, and other physical constraints [22]. As a result, these systems are generally not able to produce parts with feature sizes below several hundred microns [18, 23]. These large feature sizes allow less surface area for cells to attach and require greater amounts of time for degradation of the part to occur. Bioprinting systems, occasionally referred to as bioplotters, are subject to a similar constraint. While they are able to directly place both material and cells in a scaffold, bioplotters are limited by the nozzle diameter through which they can extrude cells [18]. As extrusion devices have difficulty with precise start/stop motion, they are limited to printing “log-cabin” cellular topologies that feature extruded serpentine paths (with large offsets between roads). In addition, thin nozzles that provide high resolution features normally result in shear stresses on cells that significantly reduce their viability. Contrary to these other AM systems, the printing resolution of vat photopolymerization is limited only by the wavelength of light and quality and tuning of optical components [17]. Mask projection microstereolithography (MP $\mu$ SL) systems able to fabricate feature sizes below  $50\ \mu\text{m}$  have been demonstrated by several groups [19, 24-27]. Such resolution would enable the fabrication of scaffold geometries with high porosity, large surface area, and pores of appropriate size for cell proliferation [28].

Tissue scaffolds must also be fabricated from material(s) that are biocompatible and biodegradable [2]. Most AM systems are not yet able to fabricate biocompatible and biodegradable materials [29]. For example, cells can be grown on scaffolds fabricated using filament-based extrusion processes, but these materials are not often easily dissolved in physiological conditions. Bioprinters, another extrusion AM process, are able to extrude a variety of natural and synthetic polymers, many of which are both biocompatible and biodegradable. Unfortunately, many of these materials have little mechanical robustness and do not serve well for large tissue scaffolds, particularly for hard tissue replacement [18, 30, 31]. In addition, bioprinters face the difficulty of keeping cells viable during the printing process, which does not usually occur in media.

Researchers have demonstrated the fabrication of tissue scaffolds with vat photopolymerization using several biocompatible synthetic polymers. These polymers often contain carbonate or ester groups that can be easily hydrolyzed under physiological conditions [32]. The most widely reported printable photopolymer for tissue scaffolds, poly(propylene fumarate) (PPF), shows good biocompatibility and demonstrates promise for use in scaffolds for hard tissue replacement [33-39]. Additional polymers reported include poly( $\epsilon$ -caprolactone) [40], poly(ethylene glycol) diacrylate [41], trimethylene carbonate [42], and poly(D,L-lactide) [43]. However, these polymers have a limited range of mechanical and chemical properties making them appropriate for tissue scaffolds for only certain types of tissue replacement. Future successes in using vat photopolymerization for the fabrication of tissue scaffolds with relevant

feature sizes hinges on the development of novel biocompatible and biodegradable photopolymers.

In an effort to expand the palette of materials from which tissue scaffolds can be fabricated, this research investigated the printability and biocompatibility of the novel polyester, PTEGA-DMA. A successful candidate material must a) permit fabrication of feature sizes below 100  $\mu\text{m}$ , b) demonstrate good cell adhesion and viability, c) exhibit mechanical properties similar to those of human tissue, and d) allow degradation in physiologically relevant conditions. To evaluate whether PTEGA-DMA is a valid candidate material for fabricating tissue scaffolds via MP $\mu$ SL, three primary research goals were devised and investigated:

- to develop process parameters for the fabrication of PTEGA-DMA tissue scaffolds using MP $\mu$ SL.
- to determine the minimum feature sizes, accuracy, and resolution that could be achieved when fabricating PTEGA-DMA parts using the MP $\mu$ SL machine.
- to gain understanding of the thermomechanical and degradation properties of PTEGA-DMA as well as assessing cell response to the material to evaluate its viability as a tissue scaffold material.

## 2. Experimental Techniques

### 2.1. Synthesis of PTEGA-DMA

Synthesis of tri(ethylene glycol) adipate was achieved through the melt polycondensation of tri(ethylene glycol) and adipic acid as described previously [44] (**Figure 2**). Functionalization to allow UV-induced crosslinking necessary for vat photopolymerization was realized through the addition of dimethacrylate end-groups via reaction of the PTEGA diol with 2-isocyanatoethyl methacrylate. Proton nuclear magnetic resonance ( $^1\text{H}$  NMR) was used to verify chemical purity of the PTEGA-DMA and determine that the product's  $M_n$  was 1,600 g/mol.

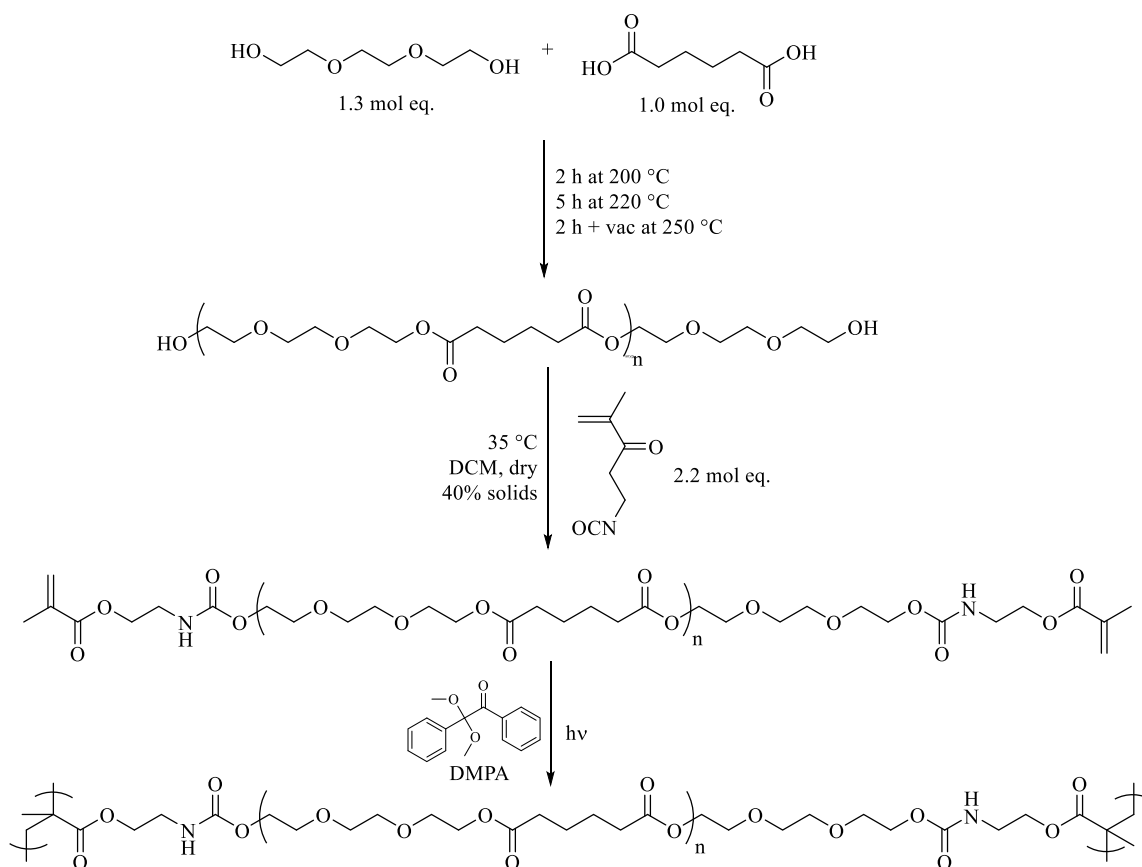


**Figure 2.** Synthesis, functionalization, and photocuring of poly(tri(ethylene glycol) adipate) dimethacrylate (PTEGA-DMA). a) melt polycondensation of tri(ethylene glycol) and adipic acid yields a poly(tri(ethylene glycol) adipate) diol. b) Functionalization of the PTEGA diol with 2-isocyanatoethyl methacrylate yields the photocurable PTEGA-DMA. c) Crosslinking through the dimethacrylate endgroups is achieved through the addition of 2,2-dimethoxy-2-phenylacetophenone (DMPA) photoinitiator and 365 nm ultraviolet light [44].

The novel polyester, PTEGA-DMA, holds a variety of advantages over other polyester compositions for use in biocompatible and biodegradable tissue scaffolds. Tri(ethylene glycol) has far reduced toxicity compared to ethylene glycol, a significantly more commonly used monomeric base in stereolithography [45]. The monomer's toxicity is important despite the lack of free monomer in oligomeric compositions used for vat photopolymerization or in fabricated parts. The hydrolysis of the polyester backbone during degradation will result in the composition reverting back to monomeric form putting cells in intimate contact with the tri(ethylene glycol). In addition, adipic acid used in the polycondensation of PTEGA-DMA has been shown to have low toxicity in rats ( $LD_{50} > 5000$  mg/kg) and is excreted in the urine [46].

## 2.2. Design of the Mask Projection Microstereolithography System

Mask Projection Microstereolithography (MP $\mu$ SL) systems have been reported to achieve resolutions and feature sizes ideal for fabricating tissue scaffolds [27, 47]. The MP $\mu$ SL machine used in this research was designed and built by Virginia Tech researchers. The top-down

projection system passes an ultraviolet LED light source (365 nm; 5.0 mJ/cm<sup>2</sup> intensity at resin surface) onto a digital micromirror device (DMD), which serves as a dynamic mask, through a series of conditioning and imaging optics, and onto a build stage mounted on a linear actuator, which dips into a resin vat (**Figure 3**). The system's DMD, a TI Instruments 1080p DLP 6500 chip, provides a 3.78 x 3.78 μm effective pixel projection size at the resin surface when implemented with the selected imaging optics. It is able to fabricate structures with feature sizes on the order of tens of microns across a build volume of up to 4 x 6 x 36 mm. The operation of the MPμSL system has been previously reported [48].

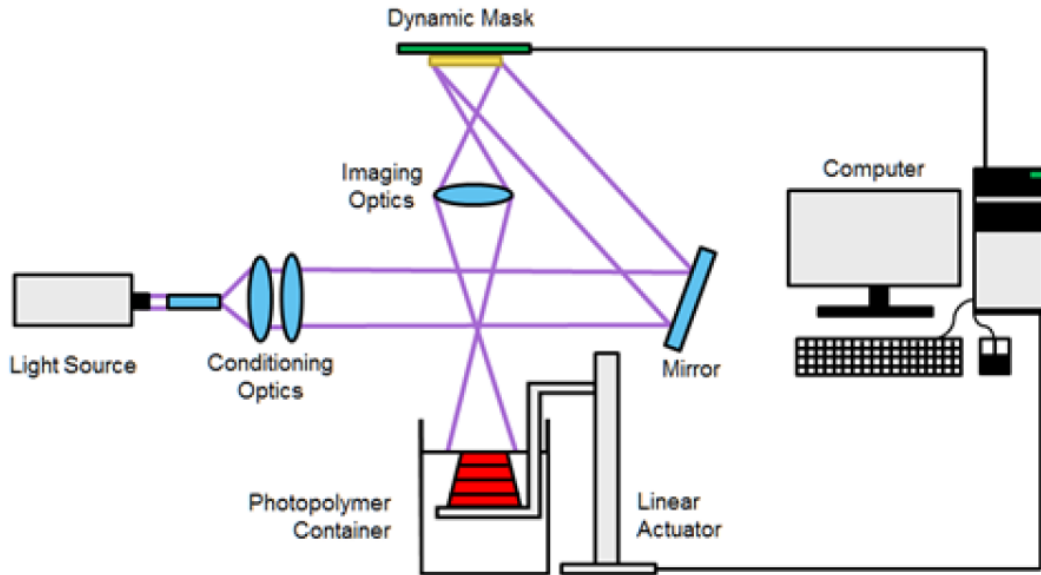


**Figure 3.** Schematic of the Mask Projection Microstereolithography machine.

### 2.3. Curing Parameters and Part Fabrication

To fabricate accurate and detailed parts using stereolithography, it is essential to understand the interaction of the photopolymer with the ultraviolet light that is curing it. As described by Jacobs, two primary intrinsic material parameters control the photocrosslinking process: the depth of penetration ( $D_P$ ) and the critical exposure ( $E_C$ ) [49]. The energy imparted to a photopolymer ( $E$ ) and the resulting thickness of the cured polymer film ( $C_D$ ) can be related to the depth of penetration and the critical exposure through the ‘Working Curve’ (Equation 1).

$$C_D = D_P \ln\left(\frac{E}{E_C}\right) \quad \text{Equation 1}$$

To determine the  $D_P$  and  $E_C$  of PTEGA-DMA, a slightly modified single-layer ‘Windowpane’ technique was used in which the build stage was removed and thin films of PTEGA-DMA were cured on the surface of the photopolymer vat surface [17]. This was repeated using several known exposure amounts and the resulting film thicknesses were tabulated. This allowed the generation of a working curve and the determination of the material’s  $D_P$  and  $E_C$ . Initial results showed that the PTEGA-DMA had a large  $D_P$ . To reduce the depth of

penetration of light into the polymer and improve resolution, avobenzone, a small molecule UV absorber often used in sunscreen, was added at 0.05 wt%.

#### 2.4. Resolution, Accuracy, and Feature Size Determination

A benchmark test part was designed and printed to quantitatively determine the resolution, accuracy, and minimum feature sizes that could be achieved using the MP $\mu$ SL machine in conjunction with the PTEGA-DMA polyester [27]. The part (**Figure 4**), has cylinders ranging from 3.5 to 150  $\mu$ m in diameter on the top surface that allow the determination of minimum feature size and resolution in the XY plane. Thin horizontal walls (20-150  $\mu$ m thick) on the sides of the part in the XZ and YZ planes reveal the resolution in these planes. The thickness of these horizontal walls as well as the thickness of the primary horizontal crossbeams help determine the extent of any undesirable crosslinking of liquid photopolymer in areas below the layer being built (also referred to as “print-through”). The XY plane accuracy can be quantitatively determined by measuring the distances between the crosshairs on the top plane of the part.

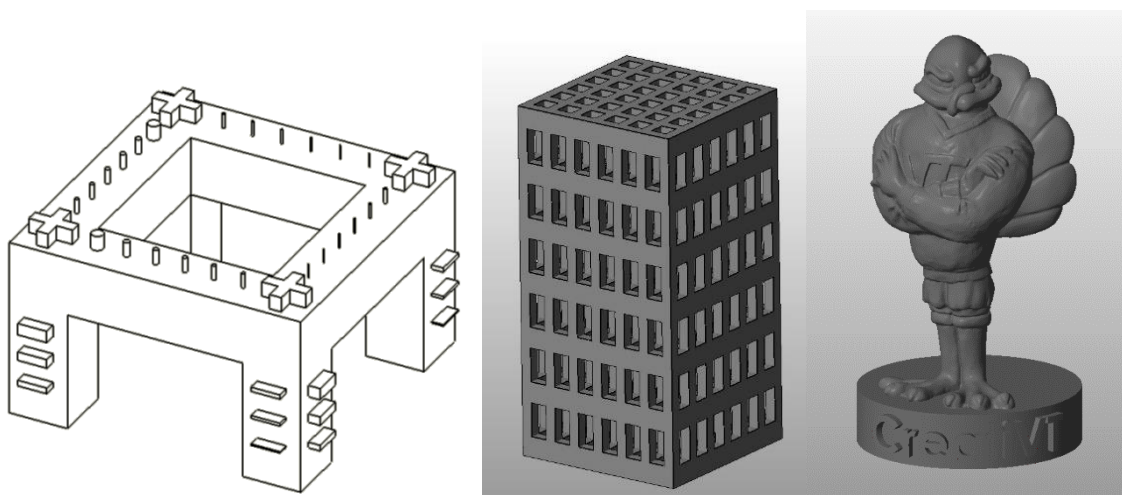


**Figure 4.** Schematic of the diagnostic test part used to determine accuracy, resolution, and minimum feature sizes that could be achieved when fabricating PTEGA-DMA parts using MP $\mu$ SL (left). To demonstrate the fabrication of complex and physiologically relevant geometries, a tissue scaffold (center) containing 400  $\mu$ m pores and a Virginia Tech Hokie bird (right) were fabricated.

To evaluate the dimensional accuracy of the test part, the samples were rinsed with isopropanol (IPA), dried, and then imaged using a Dinolight USB digital microscope. Additional images of some samples were taken with a JEOL NeoScope JCM-5000 desktop SEM. Sputter coating the samples was not necessary for SEM imaging.

#### 2.5. Characterization of Printed PTEGA-DMA Parts

In order to evaluate the feasibility of using PTEGA-DMA for the fabrication of tissue scaffolds, it is essential to understand both the thermal, mechanical and degradation properties of the material. For example, soft tissue cells respond more favorably to soft materials while cells from bone have higher viability when in contact with harder materials [50]. In addition, the

degradation of the material should happen slowly enough that cells have enough time to secrete extracellular matrix that will provide mechanical stability to the forming tissue [6].

Dynamic Mechanical Analysis (DMA) was performed to determine the glass transition temperature ( $T_g$ ) as well as the thermomechanical properties of the PTEGA-DMA at a range of temperatures. Bars of PTEGA-DMA photoinitiated with 2 wt % DMPA were printed (1.4 mm thick, 4.35 mm wide, 30 mm long) and extracted in consecutive sonicated THF and EtOH baths for 30 minutes each to remove any uncured oligomer. The bars were tested in tension on a TA Instruments Q800 DMA with a temperature ramp of 3 °C/min and a 15  $\mu$ m strain amplitude at 1 Hz. A temperature sweep between -100 °C and +100 °C determined both the  $T_g$  and the storage modulus of the PTEGA-DMA at various temperatures. The storage modulus at 37 °C was compared to those of various human tissues to determine what types of tissues and tissue scaffolds the material might be most suitable for.

The PTEGA-DMA polymer backbone contains ester bonds that can be cleaved through hydrolysis. Degradation kinetics of the polyester was determined by soaking printed scaffolds (**Figure 4**) in minimum essential media at 37 °C, for 4 h, 1 day, or 5 days. Scaffolds in media were expected to degrade at a rate similar to what would be observed in *in vivo* or *in vitro* cell culture conditions. Before soaking, the scaffolds were cleaned with IPA and vacuum dried at 50 °C for 12 hours, and weighed. After soaking in media, the scaffolds were again vacuum dried at 50 °C for 12 hours and reweighed to determine mass loss.

## 2.6. Cytotoxicity Testing of PTEGA-DMA

Cell cultures were conducted on polyester films in order to determine the cytotoxicity of the PTEGA-DMA. DMPA photoinitiator and avobenzone were dissolved in acetone and added to PTEGA-DMA at 2 wt% and 0.05 wt% respectively. Thin films were cast and photocrosslinked using a 6 W handheld UV-A lamp (Spectroline EA-160) for 5 min in a 24-well untreated polystyrene plate. The films were swelled in reverse osmosis filtered water overnight. Three 70:30 v/v EtOH/H<sub>2</sub>O extractions were performed for 60 minutes each to sterilize the films and remove any uncrosslinked oligomer. Then, two phosphate buffered saline (PBS) and one minimum essential cell media washes of 60 minutes each were used to remove residual ethanol.

MC3T3-E1 mouse preosteoblasts were cultured in minimum essential media containing 10% fetal bovine serum and 1% penicillin/streptomycin until 80% confluent. The cells were lifted from the cell culture flasks using 0.5% Trypsin-EDTA, counted, and seeded onto the PTEGA-DMA films and tissue culture treated polystyrene 24 well plates at a density of 50,000 cells/well. Cell viability was determined after 24 hours using a CellTiter-Glo luminescence assay and a BioTek Synergy Mx plate reader in absorbance mode. Viability was normalized to the tissue culture treated polystyrene plate. Cells were fixed using a formaldehyde solution (0.5% Triton X-100, 4% formaldehyde, 5% sucrose in PBS) in preparation for fluorescence imaging. 205  $\mu$ L of 165 nM Texas Red-X Phalloidin solution and 300  $\mu$ L of 300 nM DAPI (4',6-diamidino-2-phenylindole, dihydrochloride) solution, both in PBS, were added to each well. Fluorescence images were taken using a Zeiss Axio Observer.Z1 microscope.

### 3. Results & Discussion

#### 3.1. UV Curing Parameters and Part Fabrication

Using the modified Windowpane technique described in Section 2.3, the intrinsic resin properties,  $E_C$  and  $D_P$ , for PTEGA-DMA with 2 wt% DMPA were determined (**Table 1**). Due to the very large  $D_P$  of the PTEGA-DMA, parts printed without any UV blocker had significant print-through resulting in poor layer and feature definition (**Figure 5**). The addition of 0.05 wt% avobenzene dissolved in acetone served to significantly reduce the  $D_P$  and allow for the fabrication of parts with thin layers ( $<50 \mu\text{m}$ ).  $E_C$  and  $D_P$  were re-determined for the resin containing avobenzene. The increase in  $E_C$  (from 6.32 to 9.27  $\text{mJ}/\text{cm}^2$ ; a 47% increase) and decrease in  $D_P$  (from 453 to 107  $\mu\text{m}$ ; a 76% decrease) more than doubled the exposure time for curing a 50  $\mu\text{m}$  layer. However, total print time was not greatly affected as the slow recoating step contributes the largest amount of time to the print duration.

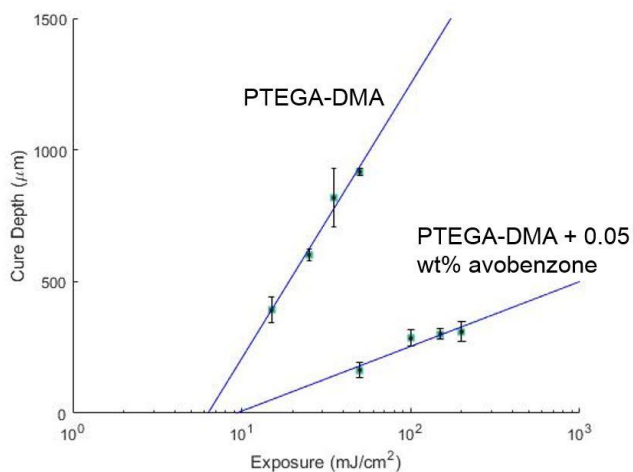


**Table 1.** Curing Parameters of the PTEGA-DMA polyester

Avobenzene concentration	0 wt%	0.05 wt%
$E_c$ ( $\text{mJ}/\text{cm}^2$ )	6.32	9.27
$D_p$ ( $\mu\text{m}$ )	453	107
50 $\mu\text{m}$ layer print time (s)	1.42	2.97

**Figure 5.** The working curve of PTEGA-DMA containing 2 wt% DMPA and 0.05 wt% avobenzene demonstrates a significantly lower  $D_p$  but slightly higher  $E_c$  than the sample without avobenzene.

To determine the accuracy and resolution that could be achieved with the PTEGA-DMA on the MP $\mu$ SL system, the diagnostic test parts described in Section 3.2 was fabricated. Parts were made using 50  $\mu\text{m}$  layer thicknesses, washed in isopropanol, and then imaged and measured using a DinoLight USB camera. The dimensions of three parts were averaged to determine minimum feature size achievable as well as the accuracy in each of the three axes. Vertical pillars with diameters as small as 30  $\mu\text{m}$  were successfully fabricated. The observed dimensions in all three axes were slightly smaller than intended (**Table 2**). This could be due to part shrinkage observed during the curing of acrylates as well as errors in the optical setup that could change the effective size of pixels on the resin surface.

**Table 2.** Printing accuracy and feature sizes achieved when fabricating the diagnostic part on the on the MP $\mu$ SL system using PTEGA-DMA.

xy accuracy	- 8.5%
xz and yz accuracy	- 3.5%
Minimum feature size (xy axis)	30 $\mu$ m

To demonstrate the fabrication of complex structures using PTEGA-DMA, a Hokie bird and tissue scaffold with square pores were built using 2 wt% DMPA and 0.05 wt% avobenzene (**Figure 6**). The 4x4x8 mm scaffold contains pores that are 400  $\mu$ m by 800  $\mu$ m. The Hokie bird is approximately 7 mm tall. Each part was printed with 100  $\mu$ m layers irradiated for 7.5 s at an intensity of 5 mW/cm<sup>2</sup>. A scaffold printed from material without avobenzene demonstrates poor resolution and feature definition. Each 100  $\mu$ m layer was irradiated for just 1.57 s.

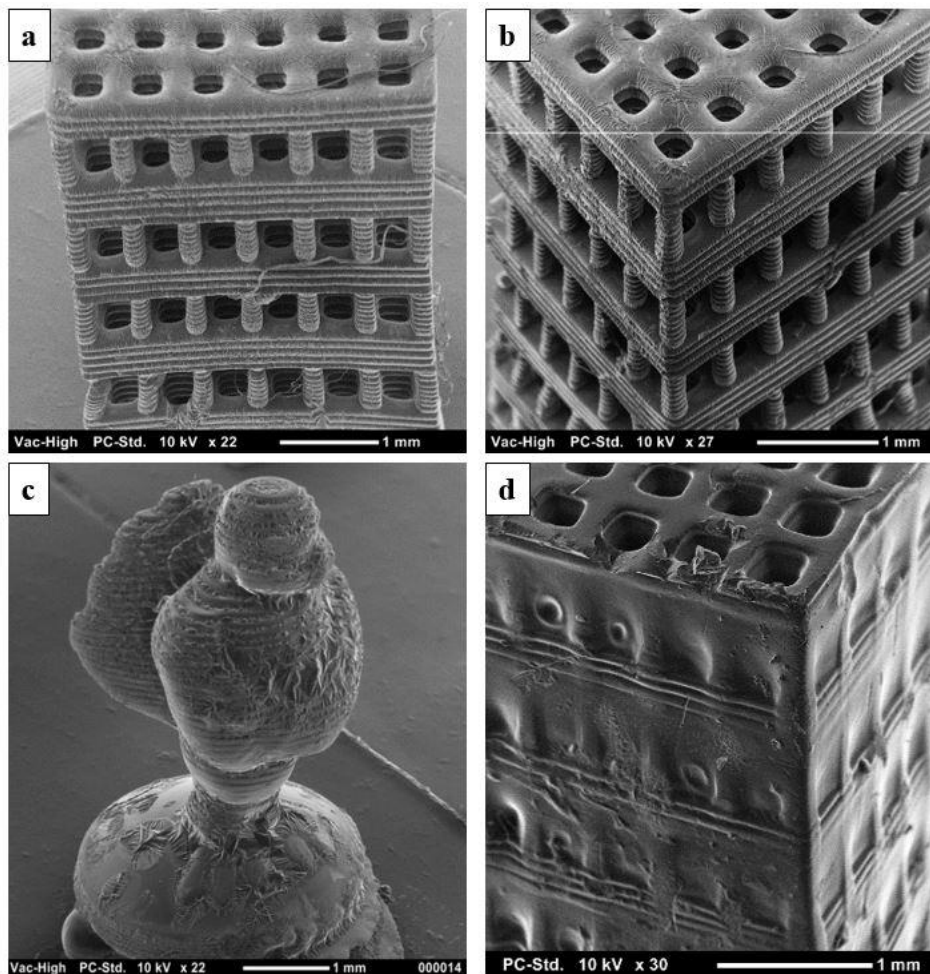


**Figure 6.** Image and SEM micrographs of PTEGA-DMA scaffolds and Hokie bird fabricated using MP $\mu$ SL. a,b,c) contain 2 wt% DMPA and 0.05 wt% avobenzene. Each 100  $\mu$ m layer was irradiated for 7.5 s at an intensity of 5 mW/cm<sup>2</sup>. d) was initiated with 2 wt% DMPA but without avobenzene. Despite the shorter irradiation time of 1.57 s per 100  $\mu$ m layer, significant “print-through” is observed.

### 3.2. Characterization of PTEGA-DMA

DMA run in triplicate showed a single phase transition and a glass transition temperature ( $T_g$ ) of PTEGA-DMA to be approximately  $3.6 \text{ }^\circ\text{C} \pm 3.6 \text{ }^\circ\text{C}$  (**Figure 7**). Because the majority of the softening occurs well below the physiological temperature of  $37 \text{ }^\circ\text{C}$ , small temperature fluctuations will have little effect on the storage modulus of the material. At  $37 \text{ }^\circ\text{C}$ , PTEGA-DMA is relatively soft and has a storage modulus of  $11.3 \pm 3.5 \text{ MPa}$ . In comparison, porcine skin has a storage modulus of approximately  $2 \text{ MPa}$  while soft spongy bone tissue found in humans have moduli in the  $40\text{-}250 \text{ MPa}$  range [51, 52]. The storage modulus of PTEGA-DMA, which falls in the range of these two tissue types, could make it a good candidate for connective tissue and spongy bone tissue scaffolds. Particularly, the incorporation of porosity in a scaffold will further reduce the storage moduli [53].

Future mechanical testing will focus on determining elastic moduli and compressive strength of both printed dogbone samples and tissue scaffolds. Testing will also be done on scaffolds after cell culture to observe how mechanical properties change with both scaffold degradation and the secretion of extracellular matrix by cells.

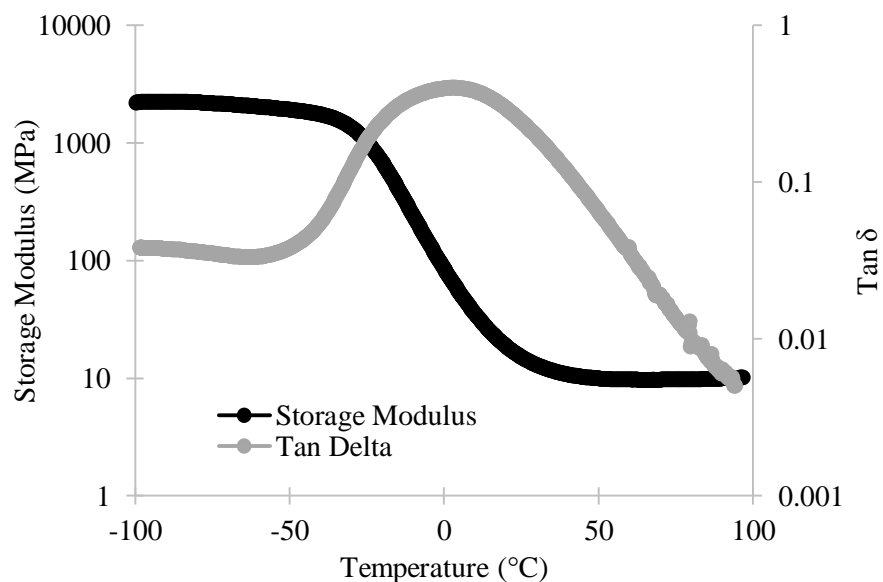


**Figure 7.** Dynamic Mechanical Analysis (DMA) reveals a  $T_g$  between at approximately  $3.5 \text{ }^\circ\text{C}$  (measured at the Tan Delta peak).

Hydrolytic cleavage of the polyester backbone occurred gradually in the presence of minimum essential media. A rapid 3% decrease in mass of the scaffolds was observed after just four hours, but the rate of mass loss slowed after this initial drop (**Figure 8**). After five days in media at  $37 \text{ }^\circ\text{C}$ , the scaffolds had lost approximately 8% of their initial mass. SEM images of the scaffolds after five days revealed that the vertical beams degraded far more than the horizontal beams (**Figure 9**). In some scaffolds, this resulted in delamination of the horizontal layers. The higher surface to volume ratio and greater number of 3D printed interfaces likely contributed to the faster degradation of the vertical beams. This testing demonstrates that the PTEGA-DMA may have the chemical robustness to provide long-term structural support in a tissue scaffold

while still permitting degradation to occur over an extended period of time. Further degradation testing will be completed at extended time points of several weeks. In addition, degradation following *in vitro* cell culture will be investigated.

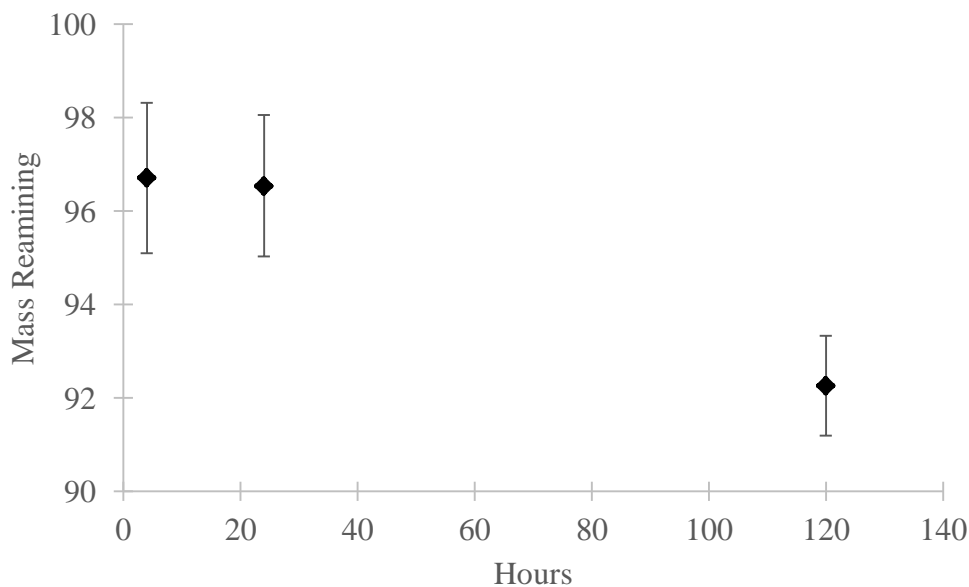


**Figure 8.** Hydrolysis testing of PTEGA-DMA showed a 3% mass loss after just four hours, but the rate of mass loss slowed after this initial drop.

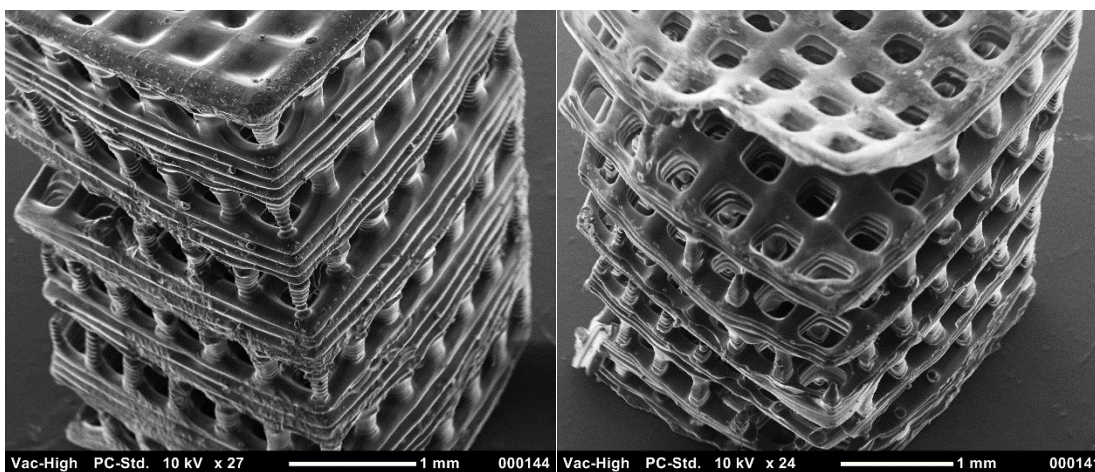


**Figure 9.** PTEGA-DMA scaffolds after 5 day soak in minimum essential media at 37 °C

### 3.3. Cell Culture and Viability

Cell viability of MC3T3-E1 mouse preosteoblasts on the PTEGA-DMA polyester films was normalized and compared to that of tissue culture treated polystyrene (**Figure 10**). After one day, cell viability on the PTEGA-DMA films was higher than on tissue culture treated polystyrene. One-way ANOVA shows that the higher cell viability of the polyester films as compared to the tissue culture treated polystyrene was statistically significant at the  $p < 0.05$  level. Texas Red

Phalloidin and DAPI staining revealed good adhesion and spreading of the cells on the PTEGA-DMA films.

Although these preliminary results are encouraging, a variety of additional tests will be performed to ensure long-term cytocompatibility of the material. Further tests will include extended time points of up to a week on films with both MC3T3-E1 preosteoblasts and 3T3 mouse fibroblasts. However, two-dimensional cell culture does not adequately replicate conditions found *in vivo*. Scaffolds similar to those demonstrated in **Figure 4** will have cells seeded on them using a perfusion bioreactor. In addition to creating a more physiologically relevant environment, this will allow the evaluation of scaffold degradation during cell culture.

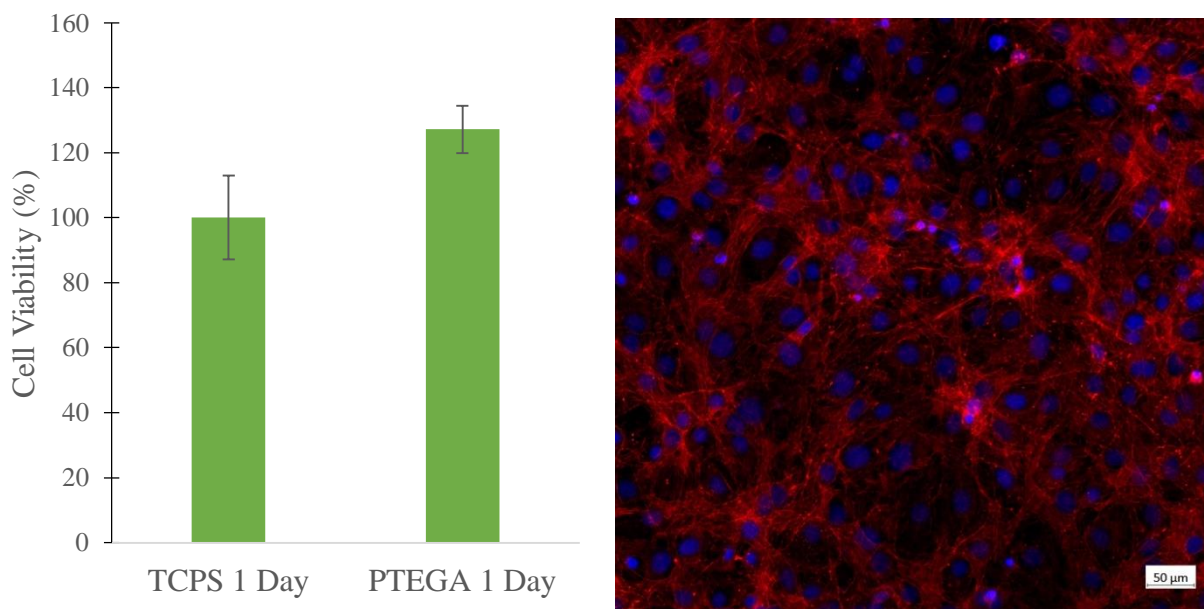


**Figure 10.** Cell viability determined via MTS assay is normalized to tissue culture treated polystyrene (TCPS). Cell viability on the polyester films were significantly higher than those on tissue culture treated polystyrene ( $p < 0.05$ ). Texas Red Phalloidin and DAPI fluorescent stains were imaged using a Zeiss Axio Observer.Z1 microscope.

#### 4. Summary and Future Work

Characterization and 3D printing of PTEGA-DMA, a novel photocurable polyester, has demonstrated that the material is a viable candidate for the fabrication of connective tissue and spongy bone tissue scaffolds using MP $\mu$ SL. With the addition of a photoinitiator and the UV absorber avobenzene, tissue scaffolds with feature sizes below 100  $\mu$ m can be fabricated using MP $\mu$ SL. In addition, PTEGA-DMA has thermomechanical properties suitable for tissue scaffolds designed for the regeneration of connective tissue and spongy bone. Cell viability studies using MC3T3-E1 mouse preosteoblasts indicate good cell adhesion and significantly higher cell viability compared to tissue culture treated polystyrene. Hydrolysis studies show that the polyester backbone degrades in minimum essential cell media but does so relatively slowly. The degradation rate observed will allow the PTEGA-DMA to provide sufficient mechanical support for developing tissue. Future work will focus on determining cell viability of both mouse

preosteoblasts and fibroblasts at extended time points. In addition, dynamic culture using a perfusion bioreactor will be employed to create a more *in vivo* like environment and allow for three-dimensional cell culture on printed scaffolds. This setup will allow the investigation that the effects of scaffold geometry (e.g. pore size and shape) have on cell response and differentiation.

## References

1. Atala, A., *Regenerative medicine strategies*. Journal of pediatric surgery, 2012. **47**(1): p. 17-28.
2. Langer, R. and J. Vacanti, *Tissue engineering*. Science, 1993. **260**(5110): p. 920-926.
3. *OPTN/SRTR 2012 Annual data report. Introduction*. Am J Transplant, 2014. **14 Suppl 1**: p. 8-10.
4. Atala, A., *Engineering organs*. Current opinion in biotechnology, 2009. **20**(5): p. 575-92.
5. Vacanti, J.P. and C.A. Vacanti, *The History and Scope of Tissue Engineering*. 2014. p. 3-8.
6. Hollister, S.J., *Porous scaffold design for tissue engineering*. Nature Materials, 2005. **4**(July).
7. Hollister, S.J., R.D. Maddox, and J.M. Taboas, *Optimal design and fabrication of scaffolds to mimic tissue properties and satisfy biological constraints*. Biomaterials, 2002. **23**(20): p. 4095-103.
8. Ronca, A., L. Ambrosio, and D.W. Grijpma, *Preparation of designed poly(D,L-lactide)/nanosized hydroxyapatite composite structures by stereolithography*. Acta Biomater, 2013. **9**(4): p. 5989-96.
9. Seol, Y.-j., et al., *Fabrication of a hydroxyapatite scaffold for bone tissue regeneration using microstereolithography and molding technology*. Microelectronic Engineering, 2009. **86**(4-6): p. 1443-1446.
10. Kim, J.Y., et al., *Development of a bone scaffold using HA nanopowder and microstereolithography technology*. Microelectronic Engineering, 2007. **84**(5-8): p. 1762-1765.
11. Badylak, S.F., et al., *Engineered whole organs and complex tissues*. Lancet, 2012. **379**(9819): p. 943-52.
12. Nguyen, L.H., et al., *Vascularized Bone Tissue Engineering : Approaches for Potential Improvement*. Tissue Engineering: Part B, 2012. **18**(5).
13. Novosel, E.C., C. Kleinhans, and P.J. Kluger, *Vascularization is the key challenge in tissue engineering*. Advanced drug delivery reviews, 2011. **63**(4-5): p. 300-11.
14. Phelps, E.a. and A.J. García, *Engineering more than a cell: vascularization strategies in tissue engineering*. Current opinion in biotechnology, 2010. **21**(5): p. 704-9.
15. Subia, B., J. Kundu, and S.C. Kundu, *Biomaterial scaffold fabrication techniques for potential tissue engineering applications*, in *Tissue Engineering*, D. Eberli, Editor. 2008. p. 141-159.
16. Lee, S.J., et al., *Development of a composite vascular scaffolding system that withstands physiological vascular conditions*. Biomaterials, 2008. **29**(19): p. 2891-8.
17. Gibson, I., D. Rosen, and B. Stucker, *Additive Manufacturing Technologies Rapid Prototyping to Direct Digital Manufacturing*. 2010: Springer.
18. Melchels, F.P.W., et al., *Additive manufacturing of tissues and organs*. Progress in Polymer Science, 2012. **37**(8): p. 1079-1104.
19. Bertsch, A., et al., *Microstereolithography: a Review*. Rapid Prototyping Technologies, 2003. **758**: p. 1-13.
20. Kang, H.W., et al., *3-D organ printing technologies for tissue engineering applications*. 2014: p. 236-253.
21. Peltola, S.M., et al., *A review of rapid prototyping techniques for tissue engineering purposes*. Ann Med, 2008. **40**(4): p. 268-80.

22. Kim, J.Y., et al., *Fabrication of a SFF-based three-dimensional scaffold using a precision deposition system in tissue engineering*. Journal of micr, 2008. **055027**.
23. Arthur, J.-h.S. and J. Kim, *Effect of solid freeform fabrication-based polycaprolactone/poly (lactic-co-glycolic acid)/collagen scaffolds on cellular activities of human adipose-derived stem cells and rat primary hepatocytes*. Journal of Materials Science, 2013. **24**: p. 1053-1065.
24. Bertsch, A., et al., *Ceramic microcomponents by microstereolithography*. Mems 2004: 17th Ieee International Conference on Micro Electro Mechanical Systems, Technical Digest, 2004: p. 725-728.
25. Cho, D.W. and H.W. Kang, *Microstereolithography-based computer-aided manufacturing for tissue engineering*. Methods Mol Biol, 2012. **868**: p. 341-56.
26. Choi, J.W., et al., *Design of microstereolithography system based on dynamic image projection for fabrication of three-dimensional microstructures*. Journal of Mechanical Science and Technology, 2006. **20**(12): p. 2094-2104.
27. Philip Lambert, Nicholas Chartrain, Alison Schultz, Shelley Cooke, Timothy Long, Abby Whittington, Christopher Williams, *Mask Projection Microstereolithography of Novel Biocompatible Polymers*, in *International Solid Freeform Fabrication Symposium*. 2014: Austin, Texas. p. 974-990.
28. Gauvin, R., et al., *Microfabrication of complex porous tissue engineering scaffolds using 3D projection stereolithography*. Biomaterials, 2012. **33**(15): p. 3824-34.
29. Yeong, W.-Y., et al., *Rapid prototyping in tissue engineering: challenges and potential*. Trends in biotechnology, 2004. **22**(12): p. 643-52.
30. Murphy, S.V. and A. Atala, *3D bioprinting of tissues and organs*. Nat Biotechnol, 2014. **32**(8): p. 773-85.
31. Xu, T., et al., *Principles of Bioprinting Technology*. 2014: p. 67-79.
32. Croll, T.I., et al., *Controllable surface modification of poly(lactic-co-glycolic acid) (PLGA) by hydrolysis or aminolysis I: physical, chemical, and theoretical aspects*. Biomacromolecules, 2004. **5**(2): p. 463-73.
33. Cho, D.-W., et al., *Estimation of cell proliferation by various peptide coating at the PPF/DEF 3D scaffold*. Microelectronic Engineering, 2009. **86**(4-6): p. 1451-1454.
34. Kempen, D.H.R., et al., *Development of biodegradable poly(propylene fumarate)/poly(lactic-co-glycolic acid) blend microspheres. II. Controlled drug release and microsphere degradation*. Journal of biomedical materials research. Part A, 2004. **70**(2): p. 293-302.
35. Lee, J.W., et al., *Development of nano- and microscale composite 3D scaffolds using PPF/DEF-HA and micro-stereolithography*. Microelectronic Engineering, 2009. **86**(4-6): p. 1465-1467.
36. Lee, J.W., et al., *Scaffold Fabrication with Biodegradable Poly(propylene fumarate) Using Microstereolithography*. Key Engineering Materials, 2007. **342-343**: p. 141-144.
37. Lee, J.W., et al., *3D scaffold fabrication with PPF/DEF using micro-stereolithography*. Microelectronic Engineering, 2007. **84**(5-8): p. 1702-1705.
38. Lee, J.W., et al., *Fabrication and characteristic analysis of a poly(propylene fumarate) scaffold using micro-stereolithography technology*. J Biomed Mater Res B Appl Biomater, 2008. **87**(1): p. 1-9.

39. Lan, P.X., et al., *Development of 3D PPF / DEF scaffolds using micro-stereolithography and surface modification*. Journal of materials science. Materials in medicine, 2009. **20**: p. 271-279.
40. Skoog, S.A., P.L. Goering, and R.J. Narayan, *Stereolithography in tissue engineering*. J Mater Sci Mater Med, 2014. **25**(3): p. 845-56.
41. Han, L.-H., et al., *Projection Microfabrication of Three-Dimensional Scaffolds for Tissue Engineering*. Journal of Manufacturing Science and Engineering, 2008. **130**(2): p. 021005-021005.
42. Lee, S.-J., et al., *Application of microstereolithography in the development of three-dimensional cartilage regeneration scaffolds*. Biomedical microdevices, 2008. **10**(2): p. 233-41.
43. Melchels, F.P.W., et al., *Photo-Cross-Linked Poly(dl-lactide)-Based Networks. Structural Characterization by HR-MAS NMR Spectroscopy and Hydrolytic Degradation Behavior*. Macromolecules, 2010. **43**(20): p. 8570-8579.
44. Sirrine, J.M., et al., *3D-Printable Biodegradable Polyester Tissue Scaffolds for Cell Adhesion*. Australian Journal of Chemistry, 2015. **68**(9): p. 1409.
45. Borron SW, Baud FJ, and G. R., *Intravenous 4-methylpyrazole as an antidote for diethylene glycol and triethylene glycol poisoning: a case report*. Veterinary and Human Toxicology, 1997. **39**(1): p. 26-28.
46. Jr., G.L.K., *Toxicity of Adipic Acid*. Drug and Chemical Toxicology, 2002. **25**(2): p. 191-202.
47. Schultz, A.R., et al., *3D Printing Phosphonium Ionic Liquid Networks with Mask Projection Microstereolithography*. ACS Macro Letters, 2014. **3**(11): p. 1205-1209.
48. Lambert, P.M., E.A.C. III, and C.B. Williams. *Design Considerations for Mask Projection Microstereolithography Systems*. in *Solid Freeform Fabrication Symposium*. 2013. Austin, Texas.
49. Jacobs, P.F. *Fundamentals of Stereolithography*. in *Solid Freeform Fabrication Symposium*. 1992.
50. Discher, D.E., P. Janmey, and Y.L. Wang, *Tissue cells feel and respond to the stiffness of their substrate*. Science, 2005. **310**(5751): p. 1139-43.
51. Ronca, D., et al., *Critical analysis on dynamic-mechanical performance of spongy bone: the effect of an acrylic cement*. Hard Tissue, 2014. **3**(1): p. 9-16.
52. Xu, F., et al. *Characterization of Thermomechanical Behaviour of Skin Tissue II. Viscoelastic Behaviour*. in *World Congress on Engineering*. 2007.
53. Moroni, L., J.R. de Wijn, and C.A. van Blitterswijk, *3D fiber-deposited scaffolds for tissue engineering: influence of pores geometry and architecture on dynamic mechanical properties*. Biomaterials, 2006. **27**(7): p. 974-85.